Applied Catalysis B: Environmental 84 (2008) 400–407

Contents lists available at ScienceDirect

Applied Catalysis B: Environmental

journal homepage: www.elsevier.com/locate/apcatb

# Relationship among the physicochemical properties, electrocatalytic performance and kinetics of carbon supported Pt catalyst for ethanol oxidation

Zhao-Hui Teng [a], Yu-Jiao Wang [a], Bing Wu [a], Ya-Wen Tang [b], Tian-Hong Lu [b], Ying Gao [a,*]

[a] Department of Chemistry, College of Physical and Chemistry, Harbin Normal University, 50 Hexing Street, Nangang District, Harbin 150080, PR China
[b] College of Chemistry and Environmental Science, Nanjing Normal University, Nanjing 210097, PR China

ARTICLE INFO

*Article history:*
Received 20 December 2006
Received in revised form 13 December 2007
Accepted 18 April 2008
Available online 29 April 2008

*Keywords:*
Carbon supported platinum catalyst
Ethanol oxidation
Electrocatalytic activity and stability

ABSTRACT

A new carbon supported Pt (Pt/C(b)) catalyst was prepared by reducing $H_2PtCl_6$ in glycol solution using formic acid as a reducing agent, and has been found in this work to be highly active and stable for the electrochemical oxidation of ethanol. The preparation produces highly dispersed Pt particles, of 2.6 nm average size, and with high electrochemical surface area, 98 $m^2/g$. The apparent activation energy of ethanol oxidation over the Pt/C(b) catalyst electrode is low, 10–14 kJ/mol, over the range of potentials from 0.3 to 0.6 V.



## 1. Introduction

In recent years, the direct methanol fuel cell (DMFC) has received increasing attention because of the ready availability and portability of methanol and its high specific energy [1–4]. DMFC is considered a possible power source for portable electronic devices and future cars. However, it has been realized gradually that DMFC has several serious problems. For example, methanol is toxic and highly flammable. The electrocatalytic activity of Pt typically used as the anodic catalyst in DMFC is low and Pt is easy to be poisoned by CO, an intermediate of the methanol oxidation. Especially, methanol is easy to cross over through the Nafion membrane, causing loss of fuel and a drop in the DMFC performance [5,6]. Therefore, many other simple organic compounds, such as ethanol [7,8], ethylene glycol [9], formic acid [10] and dimethyl ether [11], etc. have been investigated as methanol alternative fuels. Among these fuels, ethanol is considered to be an attractive and promising methanol alternative fuel [12,13], because it is very easy to be obtained by fermentation of carbohydrate-containing biomass, it is nontoxic and has a high specific energy. The main problem of ethanol as a methanol alternative fuel is that its oxidation performance is worse than that of methanol.

Generally, platinum is an excellent catalyst for the oxidation of small organic molecules, including ethanol. Many efforts have been made to prepare Pt catalysts in order to improve their electrocatalytic performance in ethanol oxidation [14,15]. It is generally accepted that the electrocatalytic performance of the Pt catalyst is strongly dependent on the shape, size and distribution of the Pt particles [16,17]. Many methods, such as microemulsion [18], microwave irradiation [19,20], solid reaction method [21], organic colloid method [22], inorganic colloid method [23], chemical reduction [24], and impregnation methods [25] have been used to prepare Pt-based catalysts. All of these preparation techniques are aimed at obtaining Pt-based catalysts with uniformly distributed Pt nanoparticles. Among these methods, the chemical reduction method is the simplest and easy to scale up. The electrocatalytic performance of different catalysts for the ethanol oxidation have been investigated by many groups [26–29]. However, only a few studies concentrated on the kinetics of the ethanol oxidation. Tarasevich et al. [30] investigated the Tafel plot, reaction order and the activation energy for the ethanol oxidation on the RuNi catalyst in alkaline electrolyte. They found two linear regions of the Tafel plot at low and high polarization ranges and described that the low slope at $E < 0.1$ V corresponds to hydrogen oxidation formed upon alcohol dehydration. Gupta and Datta [31] compared the ethanol oxidation at the Pt and PtRh catalyst electrodes and calculated the activation energy at different potentials. Only Colmati et al. [32] and Suffredini et al. [33] reported the kinetics of the ethanol oxidation at the carbon supported Pt-based catalyst electrodes.

In this work, the Pt/C(b) catalyst was prepared by reducing $H_2PtCl_6$ in glycol solution using formic acid as a reducing agent.

* Corresponding author. Tel.: +86 451 88060853; fax: +86 451 88060853.
*E-mail address:* yinggao99@126.com (Y. Gao).

0926-3373/$ – see front matter © 2008 Elsevier B.V. All rights reserved.
doi:10.1016/j.apcatb.2008.04.022

The physicochemical properties, the electrocatalytic performance and the kinetics of ethanol oxidation on Pt/C catalysts were investigated.

## 2. Experimental

### 2.1. Preparation of catalysts and electrodes

The Pt/C(a) catalyst was prepared according to Ref. [34]. The required quantity of carbon support Vulcan XC-72 activated carbon black and triply distilled water was mixed and ultrasonicated for 1.5 h. Then, the $H_2PtCl_6$ solution was added into the solution drop by drop at 85 °C for 1 h. Finally, 5 mL $NaBH_4$ (0.06 g/mL) solution was slowly added at 80 °C for 1 h to reduce $H_2PtCl_6$. The suspension obtained was filtered and washed with triply distilled water until no $Cl^-$ was detected. Finally, the slurry was dried in the vacuum condition at 25 °C. The Pt/C(a) catalyst prepared contained 20 wt.% Pt.

The preparation of the Pt/C(b) catalyst was as follows. After the required quantity of Vulcan XC-72R activated carbon black and glycol was mixed and ultrasonicated for 1.5 h, the $H_2PtCl_6$ solution was added into the solution drop by drop at 85 °C for 1 h. Then, formic acid (HCOOH:$H_2O$ = 1:1), 12 mL solution was added to reduce $H_2PtCl_6$ drop by drop at 85 °C for 1 h. The suspension obtained was filtered and washed with triply distilled water until no $Cl^-$ was detected. Finally, the slurry was dried in vacuum condition at 25 °C. The Pt/C(b) catalyst prepared also contained 20 wt.% Pt.

The commercial Pt/C catalyst from E-TEK Co. was used for comparison and denoted as the Pt/C(c) catalyst.

A certain amount of the Pt/C catalyst was dispersed in ethanol. Then, 12 μL 5% Nafion solution and 10 μL 20% PTFE suspension was mixed ultrasonically with the Pt/C catalyst slurry for 5 min. After the slurry was spread on a carbon paper and dried at room temperature in air, the Pt/C electrode was obtained. The Pt loading for all electrodes is 1.0 mg/cm$^2$. The geometrical surface area of all electrodes prepared was 0.5 cm$^2$.

The rotating disc technique was also employed to study the ethanol oxidation. The rotating disc electrode consisted of a glassy carbon rod covered by a thin layer of catalyst with a metal loading of 250 μg/cm$^2$. On the top of the catalyst covered a thin Nafion film. The geometric area of the rotation disc electrode is 0.126 cm$^2$.

### 2.2. Electrochemical measurements

The experiments were performed in a dual electrochemical cell operating in anaerobic environment. The electrochemical measurements were carried out with a CHI650A electrochemical analyzer. The scan rate was 5 or 10 mV/s. The Pt/C catalyst electrode was used as the working electrode. The Ag–AgCl electrode and Pt gauze were used as the reference and the counter electrode, respectively. All the potentials were quoted with respect to the Ag–AgCl electrode.

The solution for the electrochemical measurement was 1.0 M $C_2H_5OH$ + 0.5 M $H_2SO_4$. $N_2$ (99.999%) was bubbled into the solution for 10 min to remove $O_2$ dissolved in the solution prior to the electrochemical measurements. For the electrochemical measurement of the adsorbed CO, CO was bubbled into the solution for 10 min until CO was fully adsorbed on the electrode. Then, $N_2$ was bubbled into the solution for 10 min to remove CO in the solution. The electrochemical measurements were performed at 25 or 60 °C.

### 2.3. Physical characterization of the catalysts

Transmission electron microscopic (TEM) measurement was performed with a Tecnais G2 Twins. Before TEM examination, the sample was firstly ultrasonicated in ethanol for 20 min and then deposited onto 3 mm Cu grids covered with a continuous carbon film. The X-ray diffraction (XRD) analyses of the catalysts were carried out with an X-ray diffractometer (Japanese D/max-B) using a Cu Ka source operated at 40 keV, tube current at 30 mA. The measurement of the BET specific surface area was performed with a Malvern Company NOVA2000e instrument and the adsorption gas was nitrogen.

## 3. Results and discussion

### 3.1. Electrocatalytic performance of Pt/C catalysts for ethanol oxidation

Fig. 1 shows the linear sweeping voltammograms of 1.0 M $C_2H_5OH$ in 0.5 M $H_2SO_4$ solution at the different Pt/C catalyst electrodes at 25 °C. It is observed from Fig. 1 that there are two oxidation peaks, $p_1$ and $p_2$, at the Pt/C catalyst electrode. The potentials of $p_1$ and $p_2$ at the Pt/C(a) catalyst electrode (Fig. 1, curve a) are 0.84 and 1.20 V, respectively, while they are 0.92 and 1.24 V at the Pt/C(b) catalyst electrode (Fig. 1, curve b). The apparent current densities of $p_1$ and $p_2$ at the Pt/C(a) catalyst electrode are 96.9 and 108.4 mA cm$^{-2}$, respectively, and they are 161.8 and 154.4 mA cm$^{-2}$ at the Pt/C(b) catalyst electrode. The above result indicated that the peak potentials at the Pt/C(b) catalyst electrode are slightly more positive than those at the Pt/C(a) catalyst electrode, but the apparent peak current densities at the Pt/C(b) catalyst electrode are greatly higher than those at the Pt/C(a) catalyst electrode.

At the Pt/C(c) catalyst electrode (Fig. 1, curve c), the peak potentials are similar to those at the Pt/C(a) catalyst electrode. The apparent peak current densities are larger than those at the Pt/C(a) catalyst electrode. It is worthy to note that the apparent current density of $p_1$ is much smaller than that of $p_2$ at the Pt/C(a) and Pt/C(c) catalyst electrodes, but the apparent current density of $p_1$ is larger than that of $p_2$ at the Pt/C(b) catalyst electrode. Fujiwara et al. suggested that $p_1$ is ascribed to the production of $CO_2$ and $p_2$ is due to the formation of acetaldehyde [35]. Thus, the above results illustrate that the Pt/C(b) catalyst electrode is more effective for the deep oxidation of ethanol.

The onset potential for ethanol oxidation is an important parameter for judging the electrocatalytic activity of the Pt-based catalysts. It can be observed that the onset potentials of the ethanol oxidation at the Pt/C(a) and Pt/C(c) catalyst electrodes are almost the same (Fig. 2), but about 50 mV more positive than those at the

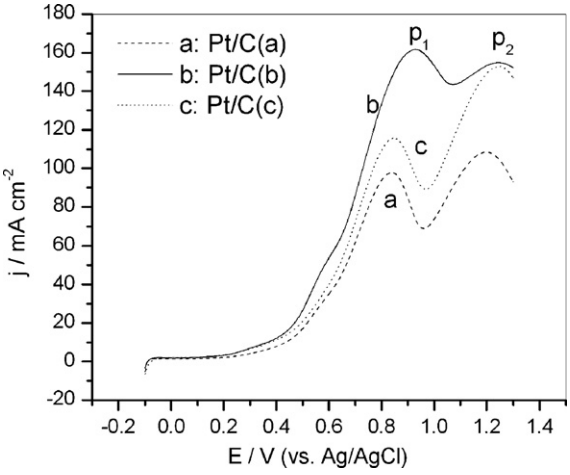


**Fig. 1.** Linear sweeping voltammograms of 1.0 M $C_2H_5OH$ in 0.5 M $H_2SO_4$ solution at (a) the Pt/C(a), (b) Pt/C(b) and (c) Pt/C(c) catalyst electrodes at 25 °C.

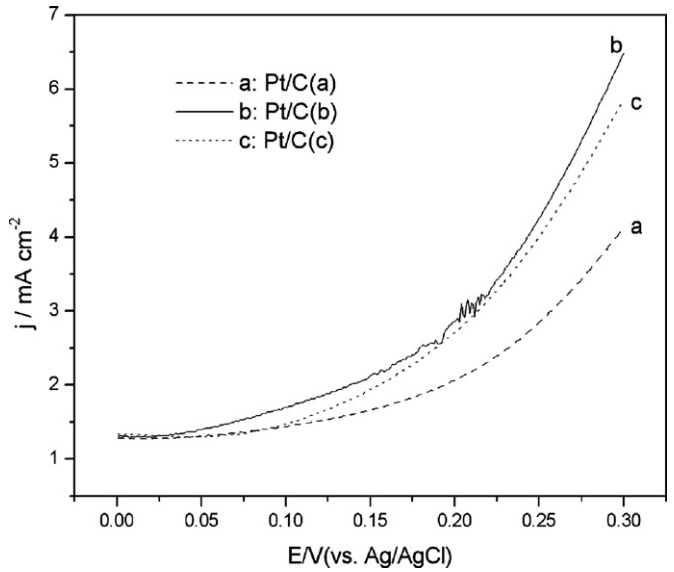


**Fig. 2.** Linear sweeping voltammograms of 1.0 M $C_2H_5OH$ in 0.5 M $H_2SO_4$ solution at (a) the Pt/C(a), (b) Pt/C(b) and (c) Pt/C(c) catalyst electrodes at 25 °C in the range of 0–0.3 V.

Pt/C(b) catalyst electrode. The results of Figs. 1 and 2 indicate the electrocatalytic activity of the Pt/C(b) catalyst electrode is much higher than that of the Pt/C(a) and Pt/C(c) catalyst electrodes for ethanol oxidation at 25 °C.

Fig. 3 shows the linear sweeping voltammograms of 1.0 M $C_2H_5OH$ in 0.5 M $H_2SO_4$ solution at the different Pt/C catalyst electrodes at 60 °C. As can be seen from Fig. 3, the oxidation peak potentials at the three catalyst electrodes at 60 °C are more positive comparing with those at 25 °C so that $p_2$ cannot be observed in the potential range of −0.1 to 1.3 V. However, the apparent peak currents of $p_1$ at the three catalyst electrodes at 60 °C are much higher than that at 25 °C. The apparent peak current densities at the Pt/C(a), Pt/C(b) and Pt/C(c) catalyst electrodes are 225, 301 and 244 mA $cm^{-2}$, respectively. The onset potential at the Pt/C(b) catalyst electrode is about 0.05 V and about 50 mV more negative than that at the Pt/C(a) and Pt/C(c) catalyst

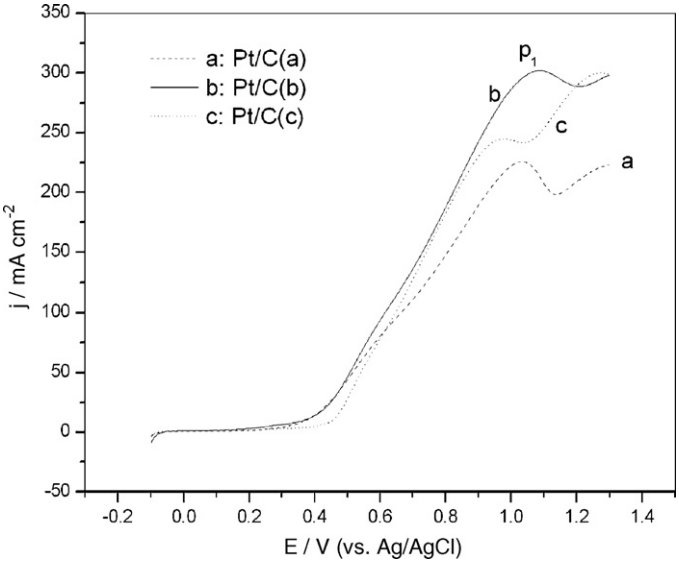


**Fig. 3.** Linear sweeping voltammograms of 1.0 M $C_2H_5OH$ in 0.5 M $H_2SO_4$ solution at (a) the Pt/C(a), (b) Pt/C(b) and (c) Pt/C(c) catalyst electrodes at 60 °C.

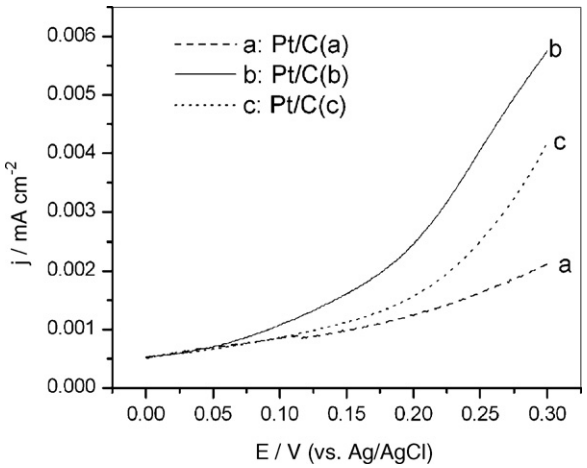


**Fig. 4.** Linear sweeping voltammograms of 1.0 M $C_2H_5OH$ in 0.5 M $H_2SO_4$ solution at (a) the Pt/C(a), (b) Pt/C(b) and (c) Pt/C(c) catalyst electrodes at 60 °C in the range of 0–0.3 V.

electrodes (Fig. 4). The above results indicate that the electrocatalytic activity of the Pt/C(b) catalyst electrode is also much higher than that of the Pt/C(a) and Pt/C(c) catalyst electrodes for ethanol oxidation at 60 °C.

### 3.2. Kinetics of ethanol oxidation over the Pt/C catalysts

Fig. 5 displays the chronoamperometry curves of 1.0 M $C_2H_5OH$ in 0.5 M $H_2SO_4$ solution on the Pt/C(a) and Pt/C(b) catalyst electrodes at different fixed potentials at 25 °C. After the initial rapid decrease in the apparent current density with time, a pseudo-steady state is achieved within 2 and 4 min for the Pt/C(b) and Pt/C(a) catalyst electrodes, respectively. It is obvious that the apparent current densities at the Pt/C(b) catalyst electrode at 3600 s are higher than those at the Pt/C(a) catalyst electrode. For example, the apparent current density at the Pt/C(b) catalyst electrode at 3600 s and at 0.7 V is about 60 mA/$cm^2$. It is only about 28 mA/$cm^2$ at the Pt/C(a) catalyst electrode. Thus, the electrocatalytic stability of Pt/C(b) is better than that of the Pt/C(a) catalyst electrode.

The long-term poisoning rate ($\delta$) can be calculated by measuring the linear decay of the current using the following equation [36]:

$$\delta\,(\%\,s^{-1}) = \frac{100}{I_0} \times \left(\frac{dI}{dt}\right)_{t>500\,s} \quad (1)$$

where $(dI/dt)_{t>500}$ is the slope of the linear portion of the current decay, and $I_0$ is the current at the start of polarization back extrapolated from the linear current decay. $\delta$ at different fixed potentials can be calculated from Fig. 5. Then, the plots of $\delta$ vs. $E$ at the Pt/C(a) and Pt/C(b) catalyst electrodes can be obtained (Fig. 6). It is clear from Fig. 6 that $\delta$ at the Pt/C(b) catalyst electrode are much lower than that at the Pt/C(a) catalyst electrode at any fixed potential. When the fixed potential is 0.7 V, $\delta$ is lowest for both catalyst electrodes. In addition, for Pt/C(a) catalyst electrode, $\delta$ increases greatly when the fixed potential is 0.8 V.

Fig. 7 shows the linear sweeping voltammograms of adsorbed CO at the Pt/C(a) and Pt/C(b) catalyst electrodes in 0.5 M $H_2SO_4$ solution at 25 °C. Three oxidation peaks of the adsorbed CO at the Pt/C(b) catalyst electrode are located at about 0.3, 0.65 and 0.87 V, indicating that there are three kinds of adsorption states of CO. However, at the Pt/C(a) catalyst electrode, only one peak at 0.65 V can be obviously observed and the peak at about 0.87 V is very

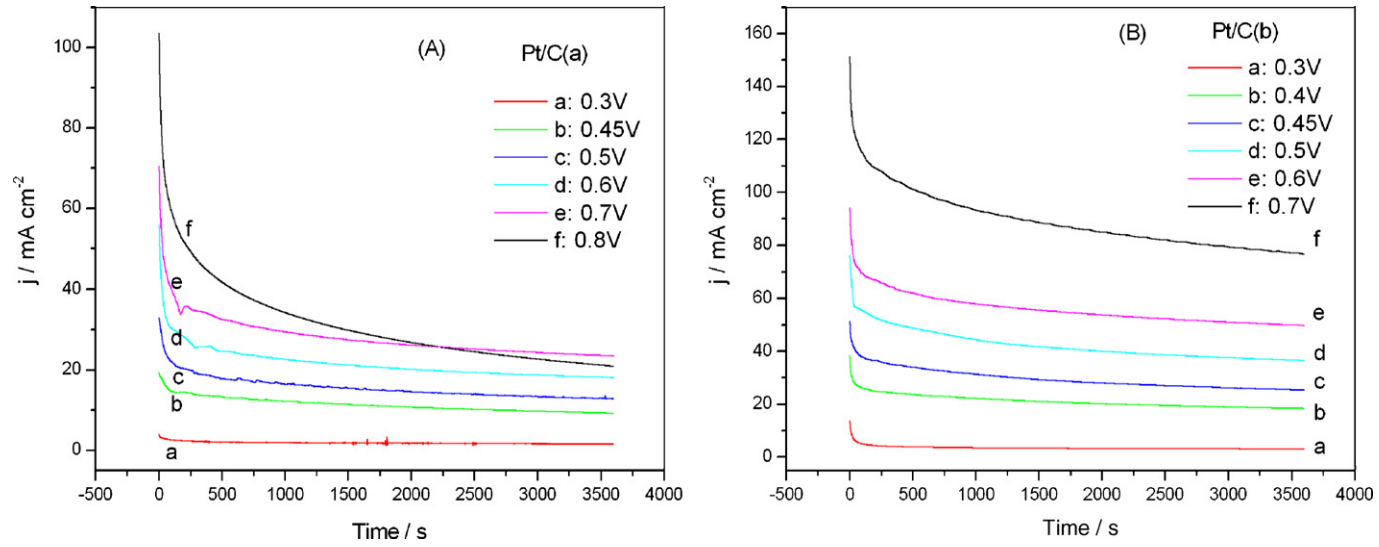


**Fig. 5.** Chronoamperometry curves of 1.0 M $C_2H_5OH$ in 0.5 M $H_2SO_4$ solution at (A) the Pt/C(a) and (B) Pt/C(b) catalyst electrodes at 25 °C. Fixed potential: (a) 0.30, (b) 0.45, (c) 0.50, (d) 0.60, (e) 0.70 and (f) 0.80 V.

small. $\delta$ may be related to the oxidation potential of the adsorbed CO. The adsorbed CO at the Pt/C(b) catalyst electrode can be partially oxidized at about 0.3 V, but no oxidation peak of the adsorbed CO at the Pt/C(a) catalyst electrode can be observed. Thus, $\delta$ at the Pt/C(b) catalyst electrode is much lower than at the Pt/C(a) catalyst electrode. Because the obvious oxidation peaks of the adsorbed CO were observed at 0.65 V at both catalyst electrodes, $\delta$ at 0.7 V is lowest for both catalyst electrodes. In addition, the oxidation peak of the adsorbed CO at the Pt/C(a) catalyst electrode at about 0.87 V is very small. Thus, $\delta$ at 0.8 V for the Pt/C(a) catalyst electrode is large.

The results mentioned above indicate that the Pt/C(b) catalyst electrode has low $\delta$, hence it possesses high CO tolerance for ethanol oxidation.

Fig. 8 displays the linear sweeping voltammograms of different concentrations of $C_2H_5OH$ in 0.5 M $H_2SO_4$ solution at the Pt/C(a) catalyst electrode. The apparent peak current density does not change appreciably with the change in the $H_2SO_4$ concentration in the range of 0.3–1.0 M when the ethanol concentration is fixed at 1.0 M. The apparent peak current density of ethanol increases with increasing the ethanol concentration (Fig. 8B). However, when the ethanol concentration is higher than 2.0 M, the apparent peak current density does not increase further. This fact can be explained by the attainment of the limiting surface coverage by the adsorbed alcohol. When the ethanol concentration is below 2.0 M, the slope of the curve of log $i$ vs. log $c_{ethanol}$ is about 0.5 (inset in Fig. 8B). Similar results were also obtained at the Pt/C(b) catalyst electrode. Therefore, the reaction order is 0.5 in ethanol.

Fig. 9 shows the linear sweeping voltammograms of 1.0 M $C_2H_5OH$ in 0.5 M $H_2SO_4$ solution at the Pt/C(a) catalyst rotating disc electrode at 5 or 10 mV/s and different rotation rates. It was found that the apparent peak current density was increased when the rotation rate was increased from 0 to 500 rpm. This means that the reaction rate is limited by ethanol transport at this condition. However, when the rotation rate is increased further, the current density is almost unchanged. In addition, the apparent peak current density is increased largely with increasing scan rate. This result indicated that the reaction rate is controlled by the diffusion and kinetics of ethanol simultaneously. Similar results were

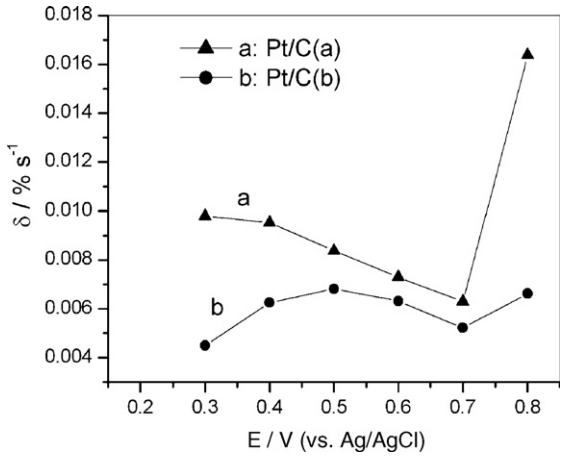


**Fig. 6.** Plots of the long-term poisoning rate ($\delta$) vs. the potential at (a) the Pt/C(a) and (b) Pt/C(b) catalyst electrodes. The current densities obtained after 3500 s polarization.

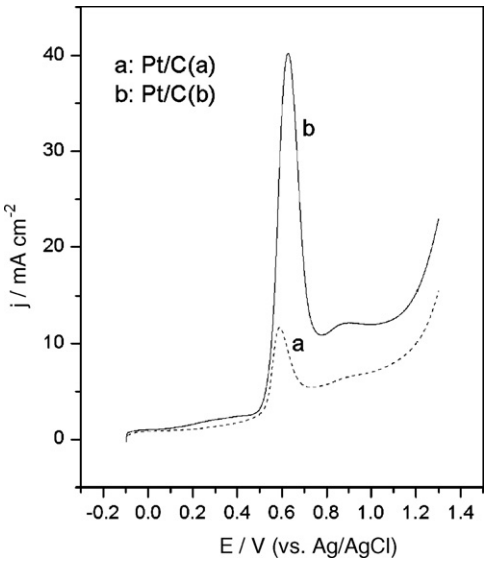


**Fig. 7.** Linear sweeping voltammograms of adsorbed CO at (a) the Pt/C(a) and (b) Pt/C(b) catalyst electrodes in 0.5 M $H_2SO_4$ solution at 25 °C.

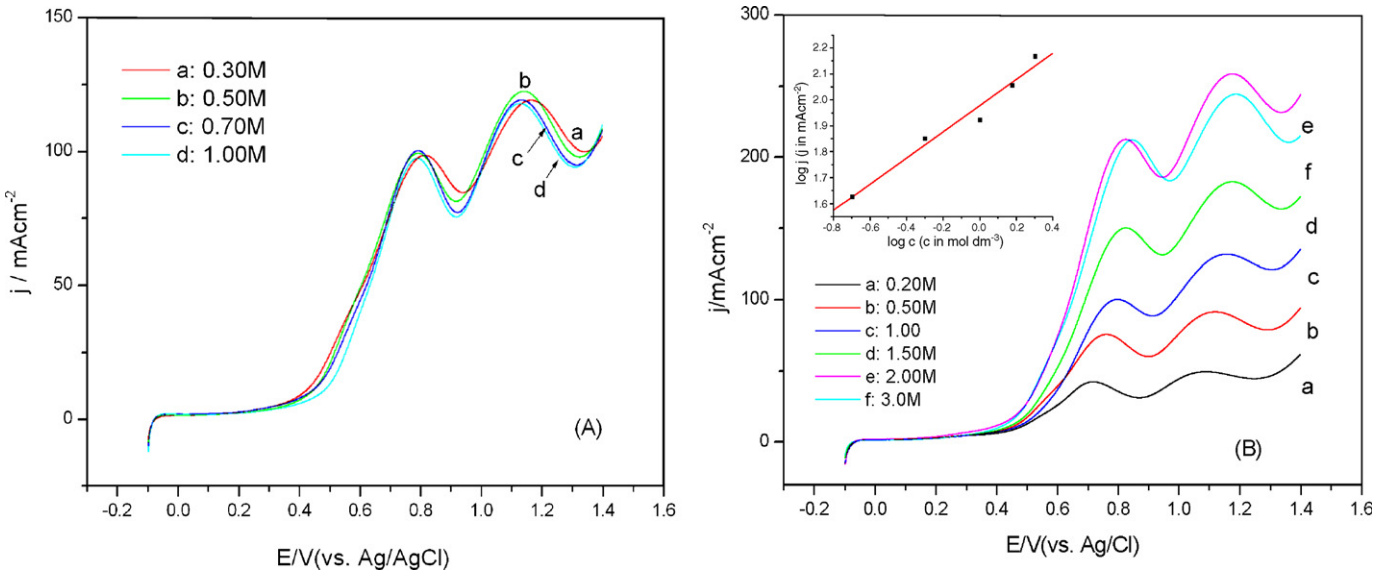


**Fig. 8.** (A) Linear sweeping voltammograms of 1.0 M $C_2H_5OH$ in (a) 0.30, (b) 0.50, (c) 0.70 and (d) 1.0 M $H_2SO_4$ solution at the Pt/C(a) catalyst electrode. (B) The linear sweeping voltammograms of (a) 0.20, (b) 0.50, (c) 1.00, (d) 1.50, (e) 2.00 and (f) 3.00 M $C_2H_5OH$ in 0.5 M $H_2SO_4$ solution at the Pt/C(a) catalyst electrode. Inset: the plot of log $j$ vs. log $c$ at 25 °C.

obtained at the Pt/C(b) catalyst rotating disc electrode. Thus, the Tafel law equation for the transport effect should be as follows [37]:

$$-\ln\left[\frac{1}{j}-\frac{1}{j_L}\right]=\frac{\alpha nFE}{RT}-\frac{\alpha nFE^{\theta}}{RT}+\ln k_0+\ln(nFc_{\text{ethanol}}) \quad (2)$$

where $j_L$ is the limiting anodic current density, $k_0$ is the standard reaction rate constant, $\alpha$ is the anodic transfer coefficient, $n$ is the number of transferred electrons. Thus, the Tafel plots of $-\ln((1/j)-(1/j_L))$ vs. the potential ($E$) at the Pt/C(a) and Pt/C(b) catalyst rotating disc electrodes at 500 rpm rotation rate can be obtained (Fig. 10). It can be seen clearly from Fig. 10 that the relationship between $-\ln[(1/j)-(1/j_L)]$ and $E$ is linear over a relatively large potential region from 0.3 to 0.65 V. According to Eq. (2), it can be calculated from the Tafel slope that $\alpha n$ is 0.30 for Pt/C(a) and 0.37 for the Pt/C(b) catalyst electrode. The value of $n$ is 2.8 for ethanol oxidation [38]. Thus, $\alpha$ is 0.11 for Pt/C(a) and 0.13 for the Pt/C(b) catalyst electrode, illustrating that the ethanol oxidation reaction at the Pt/C(a) and Pt/C(b) catalyst electrode in the acidic solution is the irreversible electrode process. For an irreversible electrode reaction, the diffusion coefficient of ethanol can be calculated according to the following equation [37]:

$$j_p = 2.99\times10^5 nc_{\text{ethanol}}(\alpha n')^{1/2}D^{1/2}\upsilon^{1/2} \quad (3)$$

where, $D$ is the diffusion coefficient of ethanol, $j_p$ is the peak current density, $\upsilon$ is the scan rate, $n'$ is the number of the transferred electrons at rate determination step. Fig. 11 represents the plots of $j_p$ vs. $\upsilon^{1/2}$ at the Pt/C(a) and Pt/C(b) catalyst electrodes in 1.0 M $CH_3CH_2OH$ + 0.1 M $H_2SO_4$ solution. It can be clearly seen

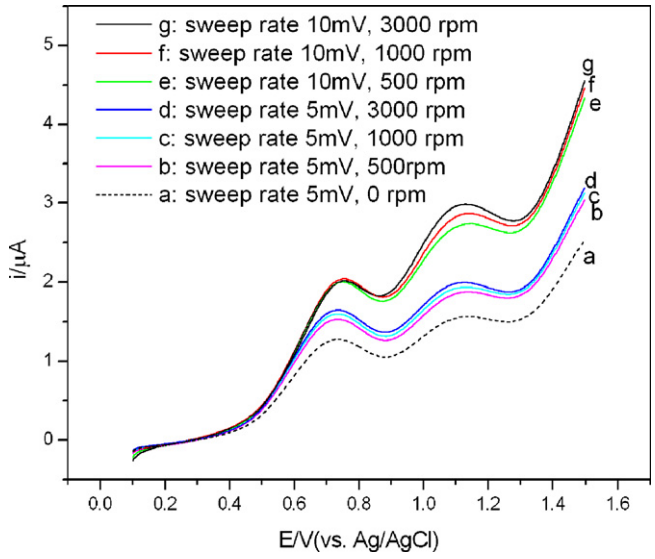


**Fig. 9.** Linear sweeping voltammograms of 1.0 M $C_2H_5OH$ in 0.5 M $H_2SO_4$ solution at the Pt/C(a) catalyst rotating disc electrode at sweep rate 5 mV/s with the rotation rate: (a) 0, (b) 500, (c) 1000, (d) 3000 rpm and at 10 mV/s with (e) 500, (f) 1000 and 3000 rpm. 25 °C.

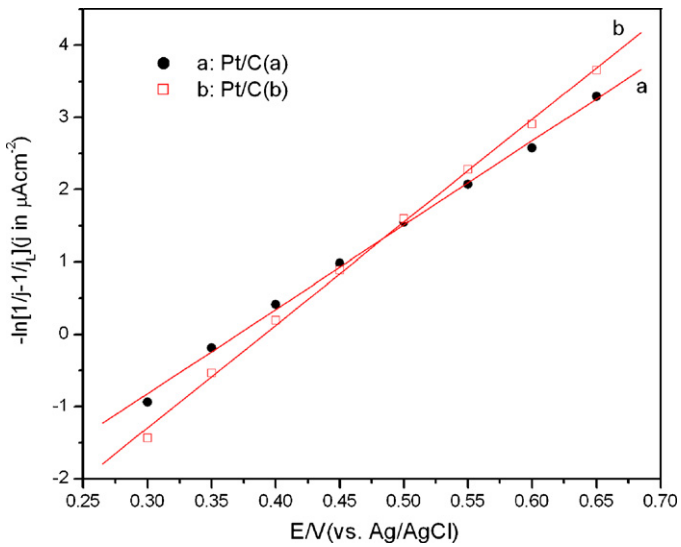


**Fig. 10.** Plots of $-\ln((1/j)-(1/j_l))$ vs. the potential at (a) the Pt/C(a) and (b) Pt/C(b) catalyst rotating disc electrodes. Electrolyte: 1.0 M $C_2H_5OH$ + 0.5 M $H_2SO_4$, rotation rate: 500 rpm. 25 °C.

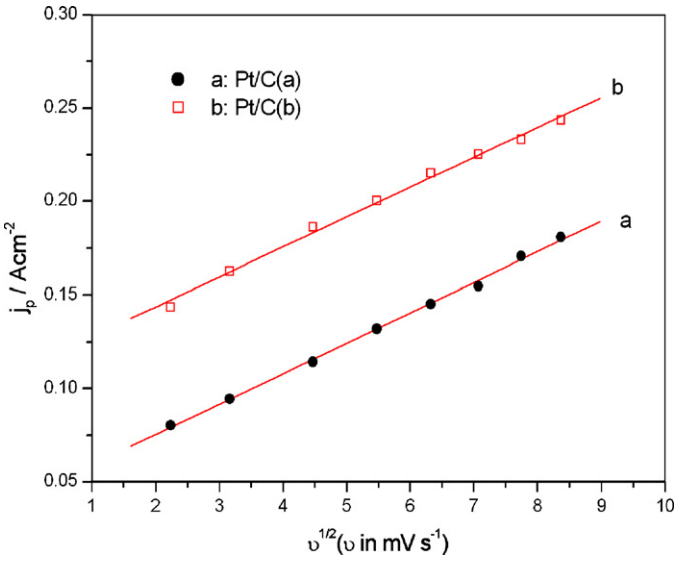


**Fig. 11.** Plots of the apparent peak current density vs. the square root of the scan rate at (a) the Pt/C(a) and (b) Pt/C(b) catalyst electrodes. Electrolyte: 1.0 M $C_2H_5OH$ + 0.5 M $H_2SO_4$ at 25 °C.

from Fig. 11 that $j_p$ and $\upsilon^{1/2}$ have very good linear relationship around the scan rate range from 5 to 70 mV/s. The value $n' = 1$, because the rate-determining step is usually one electron transfer process. The slope of the $j_p \sim \upsilon^{1/2}$ curve is 0.0163 for the Pt/C(a) catalyst electrode and 0.0160 for the Pt/C(b) catalyst electrode. Thus, the diffusion coefficient, $D$ can be calculated to be $2.3 \times 10^{-4}$ cm$^2$/s from the data either for Pt/C(a) or Pt/C(b) catalyst electrode according to Eq. (3).

Fig. 12 shows the plots of the apparent current density at different fixed potentials from 0.3 to 0.7 V at 3500 s vs. $1/T$ at the Pt/C(a) and Pt/C(b) catalyst rotation disc electrodes. It can be observed that ln $j$ is linearly proportional with $1/T$, illustrating that the reaction mechanism at each potential is not changed with temperature. The apparent activation energies, $E_a$ can be calculated at the potential from 0.3 and 0.7 V for Pt/C(a) and Pt/C(b) catalyst electrodes and the $E_a$ data are listed in Table 1. The activation

**Table 1**
Apparent activation energies of ethanol oxidation over the Pt/C(a) and Pt/C(b) catalyst electrodes

| Electrode | Apparent activation energy (kJ/mol) | | | | |
|---|---|---|---|---|---|
| | 0.3 V | 0.4 V | 0.5 V | 0.6 V | 0.7 V |
| Pt/C(a) | 10.42 | 12.66 | 13.15 | 13.44 | 26.36 |
| Pt/C(b) | 11.47 | 11.18 | 12.61 | 13.34 | 17.49 |

energy is a weak function of the potential below 0.7 V. This is similar to the result reported by Gupta and Datta [31], who found that the activation energy for ethanol oxidation at the $Pt_{90}Rh_{10}$ catalyst electrode changes from 15 to 25 kJ/mol when the potential changes from 0.35 to 0.65 V (vs. Ag/AgCl electrode). Colmati et al. [32] reported that the activation energy for the ethanol oxidation at the PtSn/C electrode changes from 40 to 50 kJ/mol with potential change from 0.35 to 0.65 V. Colmati et al. [32] also reported that the activation energy for the ethanol oxidation at the Pt/C electrode is about 27 kJ/mol when the cell voltage is 0.3–0.4 V. The reason for the dependence of the activation energy on the electrode potential is unclear and there is a variability in the results reported [30,31,32,39].

### 3.3. Structure characteristics of Pt/C catalyst

Fig. 13 displays the XRD patterns of the Pt/C(a) and Pt/C(b) catalysts. It can be observed from Fig. 13 that except for the diffraction peak of carbon (0 0 2) planes at $2\theta = 25°$, the $2\theta$ values of four characteristic peaks corresponds to (1 1 1), (2 0 0), (2 2 0) and (3 1 1) planes of the face centered cubic crystals of Pt in both XRD patterns. Thus, the Pt particles in both Pt/C catalysts possess the fcc structure. The average size of the Pt particles in the Pt/C(a) and Pt/C(b) catalysts can be calculated from the XRD pattern by means of the Scherrer equation [36].

$$d = \frac{0.9\lambda}{B_{2\theta}\cos\theta_{\max}} \quad (4)$$

where $d$ is the average size of the Pt particles, $\lambda$ is the wavelength of X-ray used ($\lambda$ = 1.54056 Å), $B_{(2\theta)}$ is the full-width at half-maximum of respective diffraction peak, and $\theta_{\max}$ is the angle at the position

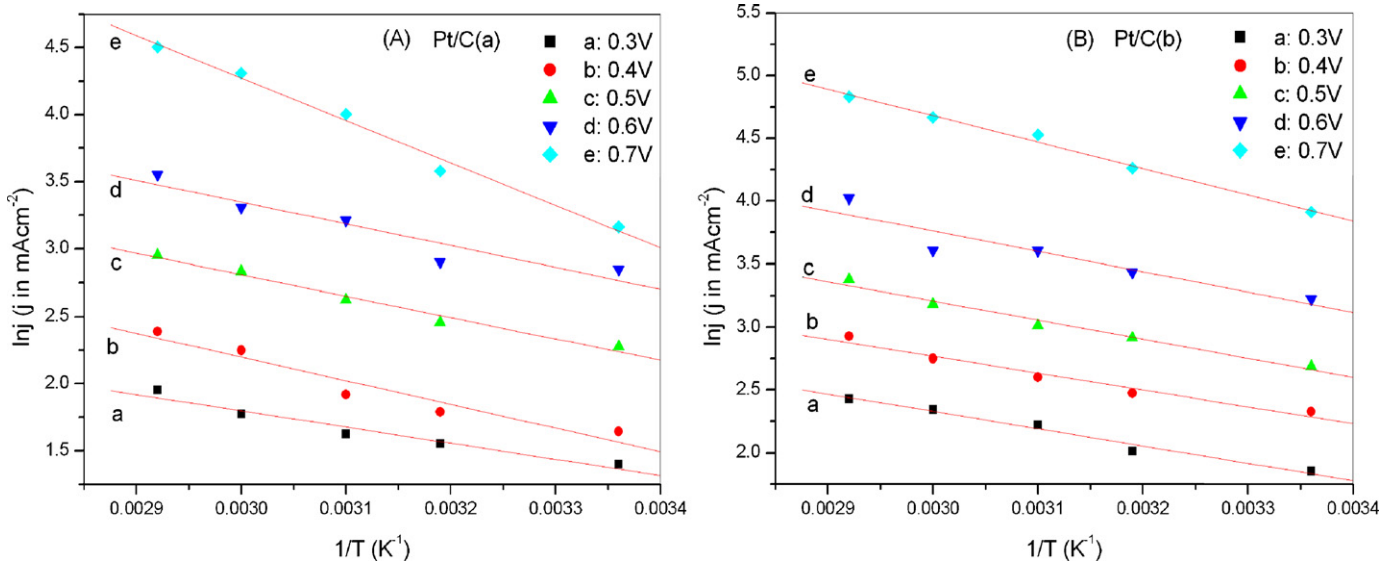


**Fig. 12.** Plots of the apparent current density at (a) 0.3, (b) 0.4, (c) 0.5, (d) 0.6 and (e) 0.7 V at 3500 s vs. $1/T$ at (A) the Pt/C(a) and (B) Pt/C(b) catalyst electrodes. Electrolyte: 1.0 M $C_2H_5OH$ + 0.5 M $H_2SO_4$ at 25 °C.

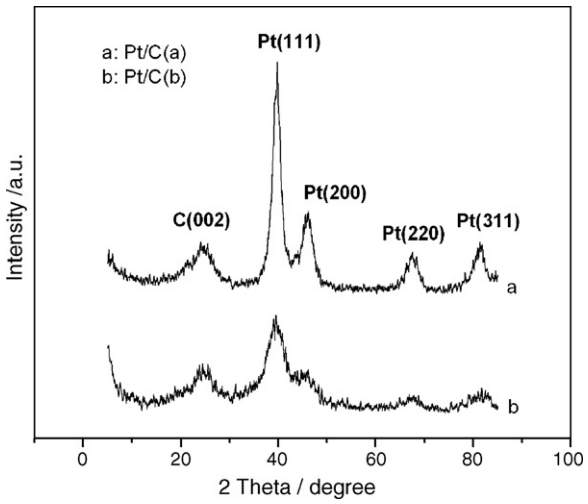


**Fig. 13.** XRD patterns of (a) the Pt/C(a) and (b) Pt/C(b) catalysts.

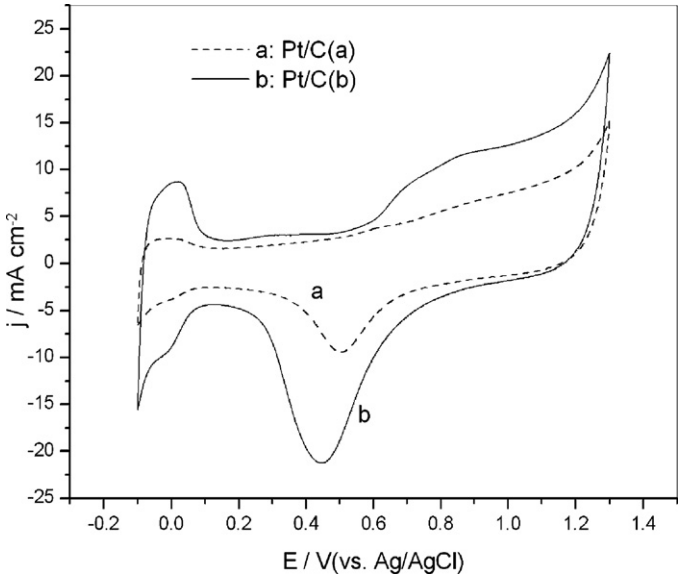


**Fig. 15.** Cyclic voltammograms of (a) the Pt/C(a) and (b) Pt/C(b) catalyst electrodes in 0.5 M $H_2SO_4$ solution at 25 °C.

of peak maximum. The Pt (2 2 0) diffraction peak was used here to calculate the Pt particle size because of its low carbon interference in the XRD pattern. The average size of the Pt particle obtained is 3.9 nm in the Pt/C(a) catalyst and 2.6 nm in the Pt/C(b) catalyst. Thus, the average size of the Pt particles in the Pt/C(b) catalyst is smaller than that in the Pt/C(a) catalyst. The specific surface area ($S_{XRD}$) can be calculated using the average size of the Pt particles and assuming a spherical shape for the Pt particles suggested by Mikhaylova et al. [40]. The $S_{XRD}$ values for both Pt/C catalysts were shown in Fig. 16.

Fig. 14 shows the TEM images of the Pt/C(a) and Pt/C(b) catalysts. It can be observed from Fig. 14 that the Pt particles in the Pt/C(b) catalyst are distributed more uniformly than in the Pt/C(a) catalyst.

Fig. 15 displays the cyclic voltammograms of the Pt/C(a) and Pt/C(b) catalyst electrodes in 0.5 M $H_2SO_4$ solution. The electrochemical specific surface area (ESA) for the Pt/C(a) and Pt/C(b) catalysts can be measured from Fig. 15 using the following equation:

$$S\,(\mathrm{m^2\,g^{-1}}) = \frac{0.1 \times Q/k}{WL} \tag{5}$$

where $W$ is the weight of the catalyst (g), $L$ is weight percent of Pt (wt.%), $Q$ is the coulometry of hydrogen desorption (mC). $k = 210\ \mu\mathrm{C/cm^2}$. The ESA values for both Pt/C catalysts are also shown in Fig. 16.

The BET specific surface area was also measured. The data of the BET specific surface area, ESA and $S_{XRD}$ of the Pt/C(a) and Pt/C(b) catalysts are shown in Fig. 16. It can be clearly seen that the BET specific surface area and $S_{XRD}$ of the Pt/C(b) catalyst is just slightly larger than that of the Pt/C(a) catalyst. However, the ESA of the Pt/C(b) catalyst is much larger than that of the Pt/C(a) catalyst. This is in good agreement with the results of the electrocatalytic activities and stabilities of the Pt/C(a) and Pt/C(b) catalysts for the ethanol oxidation. The BET specific surface area of the Pt/C catalyst includes the total surface area. However, some surface area, such as the surface area of the micropores cannot be electrochemically used. Thus, the ESA can more correctly reflect the electrochemically useful surface area.

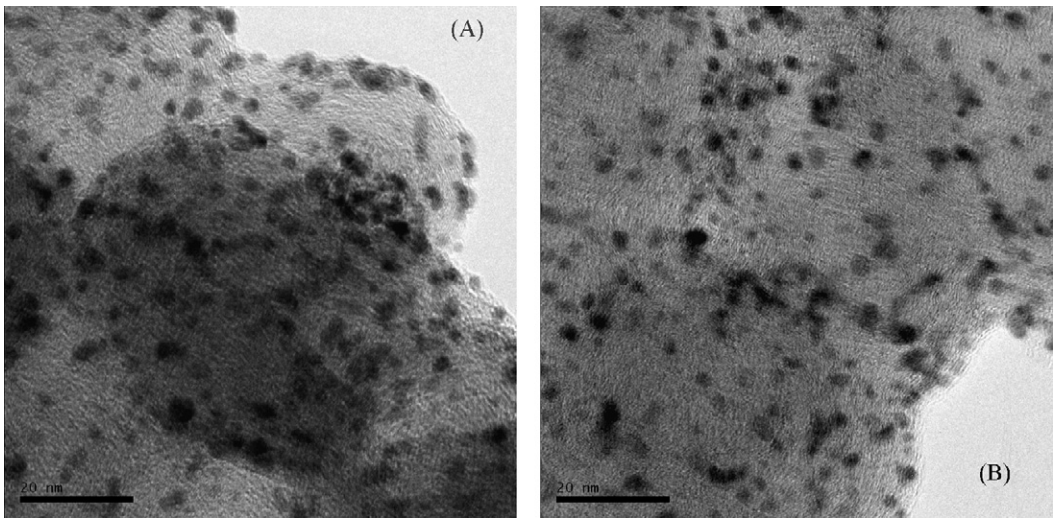


**Fig. 14.** TEM images of (A) the Pt/C(a) and (B) Pt/C(b) catalysts.

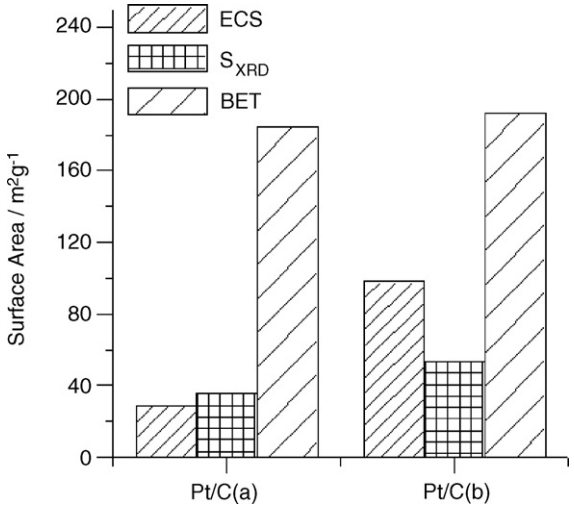


**Fig. 16.** Specific surface areas measured with the BET method, electrochemical method and the XRD method for the Pt/C(a) and Pt/C(b) catalysts.

## 4. Conclusion

The Pt/C(b) catalyst prepared by reducing hexachloroplatinic acid in a glycol solution using formic acid as a reducing agent exhibits high electrocatalytic activity and stability as well as low poisoning rate for the ethanol oxidation. This is due to the following factors. Firstly, the apparent activation energy of the ethanol oxidation at the Pt/C(b) catalyst electrode calculated from the experimental data is low, 10–14 hJ/mol at potentials of $<$0.7 V. Secondly, the XRD analysis indicated that the average size of the Pt particles in the Pt/C(b) catalyst is as small as 2.6 nm, while it is 3.9 nm for Pt/C(a). Thirdly, the TEM analysis demonstrated that the Pt particles in the Pt/C(b) catalyst are more uniformly dispersed. Fourthly, and most importantly, the ESA of the Pt/C(b) catalyst is 100 $m^2$/g, much higher than that of the Pt/C(a) (38 $m^2$/g). Hence, the dispersion of platinum is a key structural parameter in this electrocatalytic reaction.

## Acknowledgements

The authors are grateful for the financial support of 863 program (2006AA05Z137) of Science and Technology Ministry of China, the National Natural Science Foundation of China (20573029, 20573057), Natural Science Foundation of Heilongjiang Province (B200505) and Fund of Department of Science and Technology of Jiangsu Province (BK2006224), the Natural Science Foundation of the Education Committee of Jiangsu Province (05KJB150061).

## References

[1] J.F. Whitacre, T. Valdez, S.R. Narayanan, J. Electrochem. Soc. 152 (2005) A1780–A1789.
[2] E. Gulzow, M. Schulze, G. Steinhilber, J. Power Sources 106 (2002) 126–135.
[3] J.C. Amphlett, B.A. Peppley, E. Halliop, A. Sadiq, J. Power Sources 96 (2001) 204–213.
[4] K.W. Park, J.H. Choi, S.A. Lee, C. Pak, H. Chang, Y.E. Sung, J. Catal. 244 (2004) 236.
[5] W. Xu, T.H. Lu, C.P. Liu, W. Xing, Electrochim. Acta 50 (2005) 3280–3285.
[6] W. Xu, C. Liu, X. Xue, Y. Su, Y. Lv, W. Xing, T. Lu, Solid State Ionics 171 (2004) 121–127.
[7] S. Song, P. Tsiakaras, Appl. Catal. B-Environ. 63 (2006) 187–193.
[8] F. Sun, B. Wu, W.L. Qu, Y. Gao, T.H. Lu, C.P. Liu, W. Xing, Chin. J. Inorg. Chem. 21 (2005) 1546–1550.
[9] W.L. Qu, B. Wu, F. Sun, Y. Gao, C.P. Liu, W. Xing, T.H. Lu, Acta Chim. Sin. 63 (2005) 1565–1569.
[10] P. Waszczuk, T.M. Barnard, C. Rice, R. Masel, A. Wieckowski, Electrochem. Commun. 4 (2002) 599–603.
[11] G. Kerangueven, C. Coutanceau, E. Sibert, J.M. Leger, C. Lamy, J. Power Sources 157 (2006) 318–324.
[12] X. Xue, J. Ge, T. Tian, C. Liu, W. Xing, T. Lu, J. Power Sources 172 (2007) 560–569.
[13] C. Lamy, S. Rousseau, E.M. Belgsir, C. Coutanceau, J.M. Leger, Electrochim. Acta 49 (2004) 3901–3908.
[14] C. Xu, L. Cheng, P. Shen, Y. Liu, Electrochem. Commun. 9 (2007) 997–1001.
[15] C.-G. Lee, M. Umeda, I. Uchida, J. Power Sources 160 (2006) 78–89.
[16] I.S. Armadi, Z.L. Wang, T.C. Green, A. Henglein, M.A. El-Sayed, Science 272 (1996) 1924.
[17] K.A. Friedrich, F. Henglein, U. Stimming, W. Unkauf, Electrochim. Acta 45 (2000) 3283–3293.
[18] W.L. Xu, T.H. Lu, C.P. Liu, W. Xing, J. Phys. Chem. B 109 (2005) 14325–14330.
[19] Z.L. Liu, J.Y. Lee, W.X. Chen, M. Han, L.M. Gan, Langmuir 20 (2004) 181–187.
[20] Z.L. Liu, B. Guo, L. Hong, T.H. Lim, Electrochem. Commun. 8 (2006) 83–90.
[21] Y.W. Tang, H. Yang, W. Xing, T.H. Lu, Chin. Chem. Lett. 13 (2002) 478.
[22] R.-F. Wang, S.-J. Liao, H.-Y. Liu, H. Meng, J. Power Sources 171 (2007) 471–476.
[23] Y. Xu, J. Tiang, C. Zhang, Z. Shan, Chin. J. Inorg. Chem. 21 (2005) 1475–1478.
[24] E.M. Crabb, M.K. Ravikumar, Electrochim. Acta 46 (2001) 1033–1041.
[25] Y. Xu, J.H. Tian, C. Zhan, Z.Q. Shan, Chin. J. Inorg. Chem. 21 (2005) 1475–1479.
[26] J. Bagchi, S.K. Bhattacharya, J. Power Sources 163 (2007) 661–670.
[27] S. Song, W. Zhou, J. Tian, R. Cai, G. Sun, Q. Xin, S. Kontou, P. Tsiakaras, J. Power Sources 145 (2005) 266–271.
[28] G. Wu, R. Swaidan, G. Cui, J. Power Sources 172 (2007) 180–188.
[29] H. Wang, C. Xu, F. Cheng, S. Jiang, Electrochem. Commun. 9 (2007) 1212–1216.
[30] M.R. Tarasevich, Z.R. Karichev, V.A. Bogdanovskaya, E.N. Lubnin, A.V. Kapustin, Electrochem. Commun. 7 (2005) 141–146.
[31] S.S. Gupta, J. Datta, J. Electroanal. Chem. 594 (2006) 65–72.
[32] F. Colmati, E. Antolini, E.R. Gonzalez, J. Power Sources 157 (2006) 98–103.
[33] H.B. Suffredini, V. Tricoli, N. Vatistas, L.A. Avaca, J. Power Sources 158 (2006) 9–20.
[34] Z. Teng, G. Wang, B. Wu, Y. Gao, J. Power Sources 164 (2007) 105–110.
[35] N. Fujiwara, K.A. Friedrich, U. Stimming, J. Electroanal. Chem. 472 (1999) 120–125.
[36] J.W. Guo, T.S. Zhao, J. Prabhuram, R. Chen, C.W. Wong, Electrochim. Acta 51 (2005) 754–763.
[37] C.M.A. Brett, M.O. Brett, Electrochemistry, Oxford University Press Inc., New York, 2002.
[38] J. Liu, J. Ye, C. Xu, S.P. Jiang, Y. Tong, Electrochem. Commun. 9 (2007) 2334–2339.
[39] Y. Wang, L. Li, L. Hu, L. Zhuang, J.T. Lu, B.Y. Xu, Electrochem. Commun. 5 (2003) 662.
[40] A.A. Mikhaylova, E.B. Molodkina, O.A. Khazova, V.S. Bagotzky, J. Electroanal. Chem. 509 (2001) 119–127.